Author postprint version of the paper published in :
Journal of Magnetism and Magnetic Materials, volume 335, June 2013, Pages 46–52

Magnetic properties and anisotropy of orthorhombic $DyMnO_3$ single crystal

M. Pękała[a], F. Wolff-Fabris[b,c,*], J-F. Fagnard[d], Ph. Vanderbemden[d], J. Mucha[e], M. M. Gospodinov[f], V. Lovchinov[f], M. Ausloos[g]

[a] *Department of Chemistry, University of Warsaw, Al. Zwirki i Wigury 101, PL-02-089 Warsaw, Poland*
[b] *Dresden High Magnetic Field Laboratory (HLD), Helmholtz Zentrum Dresden-Rossendorf, 01314 Dresden, Germany*
[c] *MPA-NHMFL, Los Alamos National Laboratory, Los Alamos, New Mexico 87545, USA*
[d] *SUPRATECS, Department of Electrical Engineering and Computer Science B28, University of Liege, Sart Tilman, B-4000 Liege, Belgium*
[e] *W. Trzebiatowski Institute for Low Temperature and Structure Research, Polish Academy of Science, PO Box 1410, 50-950 Wrocław 2, Poland*
[f] *Institute of Solid State Physics, Bulgarian Academy of Sciences, 72 Tzarigradsko Chaussee blvd, 1784 Sofia, Bulgaria*
[g] *SUPRATECS, Department of Physics B5a, Sart Tilman, B-4000 Liege, Belgium*
[*] *now at European XFEL GmbH, Notkestrasse 85, 22607, Hamburg, Germany*

Keywords: manganites, magnetization, magnetic anisotropy

ABSTRACT

An orthorhombic $DyMnO_3$ single crystal has been studied in magnetic fields up to 14 T and between 3 K and room temperature. The field dependent ordering temperature of Dy moments is deduced. The paramagnetic Curie Weiss behavior is related mainly to the Dy^{3+}sublattice whereas the Mn sublattice contribution plays a secondary role. DC magnetization measurements show marked anisotropic features, related to the anisotropic structure of a cubic system stretched along a body diagonal, with a magnetic easy axis parallel to the crystallographic *b* axis. A temperature and field dependent spin flop transition is observed below 9 K, when relatively weak magnetocrystalline anisotropy is overcome by magnetic fields up to 1.6 T.

1. Introduction

Manganites are manganese compounds of composition AMnO3, where e.g. A= La, Ca, Ba, …, which crystallize in the cubic structure of the so called "perovskite mineral" $CaTiO_3$. Depending on the composition they show a wide variety of magnetic and electric phenomena, including ferromagnetic, antiferromagnetic, charge and orbital ordering. The multiferroic behaviour and magnetoresistive effects make such oxides as natural candidates for potential spintronics applications [1,2]. Intrinsic anisotropy is induced if the A site is occupied by different types of ions, with e.g. different intrinsic charges. When the site A is partially or fully occupied by a magnetic ion, a severe intrinsic anistropy may be induced and the compounds show different anisotropic behaviors as the temperature is changed. This is much so if the A ion has an f-shell, like in the rare earth ions. It is easily guessed that such anisotropic features will surely depend on the orientation of any applied magnetic field.

The perovskites manganites where A is a rare-earth (RE) element present the coexistence of magnetism and ferroelectricity. Moreover, either orthorhombic or hexagonal $REMnO_3$ exhibit multiferroicity but with different origin for the spontaneous polarization in these two symmetries. In the hexagonal case the structural distortions which raise from an asymmetric oxygen coordination around the RE element leads to a polarization [3] while in the orthorhombic $REMnO_3$ compounds the ferroelectricity is linked to an inversion symmetry breaking due to a complex spiral spin order [4,5]. Furthermore orthorhombic materials present a rich variety of phase diagrams and physical phenomena which endure a matter of intensive studies and discussions [6,7,8,9]. Among these multiferroic manganites, $DyMnO_3$ seems to be the least studied in either orthorhombic or hexagonal crystallographic phases, even though it had been synthesized as far back as 1984 [8]. The main challenge for studying these manganites is likely the great difficulty to grow good quality single crystals [10] where the orthorhombic phase of $DyMnO_3$ has the advantage to be chemically stable at room temperature in contrast to the high temperature hexagonal $DyMnO_3$ [11]. Furthermore, $DyMnO_3$ grows in both crystalline structures with remarkably distinct physical properties [12,13,14,15] and recently the sinusoidal spin ordering in $DyMnO_3$ has been proposed to be phenomenologically described by the Heisenberg model [16] in the orthorhombic case.

The complexity of the physical phenomena related to the anisotropic effects and the crystalline structure in manganites brings us the opportunity to present a detailed study of the magnetic properties of an orthorhombic $DyMnO_3$ single crystal.

In this article we present and discuss results on the ordering regimes and microscopic properties based on magnetization experiments down to low temperatures and high magnetic fields up to 14 T when applied in the *bc* crystallographic plane.

2. Synthesis and experimental details

Differently to the method of Kamegashira [8], the $DyMnO_3$ single crystals were grown by a high temperature solution method using a Pb_3O_4: PbF_2: B_2O_3 = 0.84: 0.14: 0.01 flux, as done previously for other $REMnO_3$ manganites [13]. The flux was mixed with $DyMnO_3$ powder in a 9:1 ratio and annealed in a platinum crucible at 1280 ^oC for 48h. After that the temperature was decreased down to 930^oC at a rate of 0.5^o C/h. The flux was decanted and well-shaped plate-like crystals were removed from the crucible. The crystallographic and electrical characteristics of the crystals are discussed in the next section.

The DC magnetization measurements as a function of temperature and magnetic fields were performed in a 14 T Quantum Design PPMS using the vibrating sample magnetometer option. The magnetic measurements include zero field cooled (ZFC) and field cooled (FCC) procedures in a temperature interval ranging from 3 K up to 350 K. The anisotropic studies were carried out by applying at first a magnetic field along the crystal face considered to be

one edge parallel to the crystallographic *b* axis in the *b*-*c* plane. The orientation of the sample was subsequently varied as related to the applied magnetic field from the original axis, so called the reference zero degree angle (B // *b*) up to 90 degrees, by rotating the sample around the *a*-axis such that one considers the final field direction as being for B // *c*.

3. Structural and electrical characterization

X-ray diffraction measurements were performed on one $DyMnO_3$ single crystal having dimensions of approximately 1.1 x 1.2 x 5.1 mm^3 and weighting 45.84 mg. The quality of the sample from a crystallographic and purity point of view is confirmed by the lack of any traces of which could be found in the X-ray diffraction patterns (Figure 1). The sample was measured at room temperature on a powder X-ray diffractometer DRON 3M (Fe-filtered Co K_α radiation) in the 2Θ interval between 20-60 degrees and the Bragg peak indexes referring to the $DyMnO_3$ are indicated. The unit cell parameters were refined using PDI package [17] and we have found that a=0.5272 (2) nm, b=0.5795 (2) nm, c=0.7380(4) nm and consequently V= 0.22547(3) nm^3. These parameters agree well with values reported for the orthorhombic phase (space group-Pbnm(62)) of the single poly- and nano-crystalline manganites [14,18,19,20,21,22]. However one may interestingly notice that both *a* and *b* unit cell parameters of the crystal studied are shorter than those reported for the poly- and nano-crystalline $DyMnO_3$. A more detailed spectroscopy study is found separately [23].

Furthermore, let us first observe that this $DyMnO_3$ single crystal is a poor electrical conductor material. As an additional characterization the electrical resistance (Figure 2A) measured along the longest sample edge (*c* axis) is relatively high (in the order of 40 Ω.cm) at room temperature and as the temperature is cooled down a semiconducting type behavior is observed. The electrical resistance even increases by four orders of magnitude, when the temperature is lowered from 300 K down to 200 K. Such a behavior reveals increased electron localization and is consistent with a low temperature transition towards a phase

having a spontaneous electrical polarization [20]. The electrical resistivity follows the simple small polaron model [19] $R(T) = R_0 T e^{E_A / k_B T}$ in the temperature interval between 220 and 300 K and may be fitted with a 0.33 eV activation energy (Figure 2B). Such an activation energy is comparable to the values reported by Pena et al. [25] for a $Dy_{1-x}Ca_xMnO_3$ ($0.00 < x < 0.60$) solid solution.

4. Low field magnetization

Figure 3 shows the temperature dependence of the DC magnetization for several directions of the applied magnetic field rotated in the *b*-*c* plane, i.e. varied from 0^o (B//*b*) to 90^o (B//*c*) under applied magnetic fields of 0.05 T, 1 T or 5 T. The corresponding angular dependences of the magnetization at fixed temperatures are plotted in figure 4. As can be seen from figure 3, the DC magnetization magnitude of the $DyMnO_3$ single crystal raises monotonically with the magnetic field strength as the temperature is lowered. The temperature dependence of the DC magnetization measured with an applied magnetic field in the *b*-*c* plane reveals a large magnetic anisotropy, as demonstrated when the magnetic field points towards *c* axis (figure 4).

Before discussing more details on these results one should first consider whether a demagnetization correction factor extrinsic effect can be influencing the obtained data. In our experiment, the magnetic field is initially applied perpendicularly to the longest direction of the single crystal. The sample is therefore magnetized by the applied field B_0 and the field produced by the resultant magnetic poles in the sample body, i.e. the demagnetizing field B_d. Using the data plotted in figures 3 and 4, the apparent magnetic susceptibility $\chi_{ext} = M / B_0$ lies approximately in the range 0.01-0.3. The demagnetization factor is hereby determined using the analytical expressions derived for rectangular prisms in the limit $\chi = 0$ [26,27,28], since the χ dependence of the demagnetization factor in this range is rather small [29]. In

addition we consider the demagnetizing field averaged over the sample volume, defined by the dimensionless magnetometric demagnetization factor N_m. This factor is calculated to be $N_m = 0.426$ for B//b and $N_m = 0.4708$ for B//c in the case of our single crystal. The intrinsic magnetic susceptibility of the sample, χ, can be determined from the measured quantity χ_{ext} as follows:

$$\chi = \frac{\chi_{ext}}{1 - N_m \, \chi_{ext}} . \qquad (1)$$

A correction of the measured data using the above formula is only relevant for the highest values of the susceptibility, e.g. for $\mu_0 H_0 = 1$ T // b (0°) at T = 10 K, one has $\chi_{ext} = 0.235$ and the corrected intrinsic susceptibility χ equals 0.261. This corresponds, however, to a relative increase of only ~ 11 %, which is quite smaller than the anisotropic behaviour effect depicted in figures 3 and 4. For *B* // c, the demagnetizing factor is somewhat higher than for *B* // b, but since the amplitude of the susceptibility is substantially smaller we conclude the demagnetization correction is negligible (~1%). Although the demagnetization corrections cannot be determined analytically for intermediate angular positions between 0° and 90°, the orders of magnitude of corrections mentioned above do clearly show that the anisotropic behaviour observed in this work results from the intrinsic anisotropy of the single crystal and not from extrinsic demagnetization effects due to the particular shape of the crystal.

The magnetization curves measured at magnetic field angles varying from *b* to *c* axis evolve gradually. In particular, when the magnetic field is applied along the *c* axis no magnetic transition is observed above 3 K and a simple Curie-Weiss type variation magnetization is seen both for the 0.05 and 1 T magnetic fields. The magnetic behaviour is different when the magnetic field is oriented along the *b* axis: a maximum in the magnetization is found at some temperature which we thereby define as the Néel temperature T_N of the Dy moment ordering. The Néel temperature of the single crystal shifts down from 7.5 to 6 K when the magnetic field is raised from 0.05 to 1 T. The magnetization maximum

seems to shift even below 3 K when 5 T is applied along *b* direction. This measured T_N value falls absolutely into the interval from 5 to 9 K reported for single crystals [12,13,18,20,30], poly- and nanocrystalline $DyMnO_3$ [19,25,30]. These differences in T_N values may be due to the structural and magnetic disorder at the crystallite surface layers, structural quality and/or oxygen stoichiometry of samples. However values of T_N are only weakly dependent on the magnetic field orientation when going from 0^o to 70^o in the *b*-*c* plane, whereas T_N disappears above 80^o, i.e, when approaching the *c* axis. These results suggest that the antiferromagnetic ordering does not develop along the *c* axis. One may also remind that a T_N as high as 17 K was reported for polycrystalline $DyMnO_3$ [31].

The magnetization at selected temperatures is compared for both 0.05 and 1 T cases as a function of the magnetic field orientation angle in figure 4. At low magnetic field (0.05 T), the magnetization maximum is located between the 10^o and 30^o angles depending on the temperature, while in the stronger (1 T) field, the magnetization maximum appears at 10^o for all studied temperatures. Additionally we also observe a pronounced slope change around 60^0 for the curves at 4, 10 and 20K. This behavior can reflect both structural and magnetic anisotropy when the applied field direction changes from *b*-axis to *c*-axis. Note that when computing the square of the ratio of the unit cell parameters *c*/*b*, this gives approximately a value of 1.6218. Calculating the $\tan^{-1}$ of 1.6218 it is found that it corresponds to an angle equal to 58.34^0 where a slope change can be observed in figure 4. This agreement may also indicate a regime change, i.e. near this value, where the ratio of energies (i) the product between the magnetic field times the spin value along c-axis and (ii) the spin-spin exchange interaction energy on the ab plane changes from below 1 to above 1. In other terms, above this angle, the interaction along the c-axis becomes dominant as compared to the exchange interactions on the ab plane.

5. Paramagnetic susceptibility

In order to analyze the paramagnetic phase of the $DyMnO_3$ single crystal, the magnetic susceptibility $\chi(T)$ was derived from measurements performed under 0.05 T and 1 T magnetic field (Figure 5) following the sample rotation around the *a* axis.

The room temperature data of the magnetic susceptibility $\chi(T)$ are found to be dependent on field and its direction: $\chi(T)$ is about 20 % higher along the *c* axis than the *b* axis both at 0.05T and 1 T. Moreover the room temperature magnetic susceptibility measured in 1 T magnetic field is about 30 % larger than that of the 0.05 T case.

The temperature variation of the inverse magnetic susceptibility displays some gradual evolution in the slope at low temperatures, when changing the magnetic field direction from the *b* to *c* axis. One may distinguish two different families of $1/\chi(T)$ plots corresponding to the vicinity of 0^o and 90^o, respectively. For the sake of clarity, the curves overlapping at intermediate field orientations are not plotted. The minimum observed in the temperature variation of the inverse magnetic susceptibility when the field orientation angle ranges from 0^o and 80^o, separates the low temperature antiferromagnetic phase from the paramagnetic one. On the contrary no minimum in $1/\chi(T)$ is observed when the magnetic field is parallel to the *c*–axis (90^o). The almost linear shape of the $1/\chi(T)$ plot shows that the Curie-Weiss law

$$\chi(T) = \frac{C}{T - T_W}, \qquad (2)$$

where T_W stands for the Weiss temperature and C is the Curie constant, is obeyed above 50 K for all magnetic field orientations. In turn, an evolution of $1/\chi(T)$ plots results in a variation of T_W and C.

It is worth to notice that the Weiss temperatures Tw, derived from data above 50 K, are negative for all magnetic field orientations (figure 6), which implies an overwhelming tendency towards antiferromagnetic interactions in the system containing the Mn and Dy

magnetic moments. It is worth to emphasize that this interaction is considerably stronger along the *c* axis (T_W is about -150 K) than along the *b* axis, with T_W close to zero. One may recall that an intermediate value, about -25 K, was found for polycrystalline [25] and nano-crystalline [19] $DyMnO_3$.

On the other hand, the effective magnetic moment μ_{EF} per formula unit derived from the Curie constant C is plotted for different sample orientations in figure 7. When the magnetic field is along the *b* axis or tilted up to 50^o towards the *c* axis, the values of μ_{EF} lie between $10.7\mu_B$ and $10.9\mu_B$ being very close to the free Dy^{3+} ion value of $10.65\mu_B$**.** Our findings reveal that an additional contribution from the Mn sublattice is negligible or self-compensated. This observation is in some contrast to that reported for other cases [19,25], i.e. in poly- and nano-crystalline $DyMnO_3$, where the μ_{EF} values reached about $11.5\mu_B$ and are related to the Mn magnetic moments.

Furthermore, when the magnetic field is tilted by 60^o up to 80^o in direction of c axis, the values of μ_{EF} are found to be lower than $10.5\mu_B$, which may point to a partial compensation of the Dy and Mn magnetic sublattices. Such a behavior may be interpreted as resulting from a negative (antiferromagnetic) interaction between the Dy and Mn ions on their sublattices. Nevertheless the highest effective magnetic moment thereby deduced, $11.7\mu_B$, is observed to occur along the *c* axis (90^o); thus it may be argued that it also results from some contribution from the Mn ions. It is worth to notice that a so high value of μ_{EF} corresponds with the strongest antiferromagnetic interaction revealed by the Weiss temperature value discussed previously.

6. High field magnetization

In order to investigate some possible magnetic hysteresis, in view of technological applications of this compound, magnetization loops were registered under a magnetic field varying between 14 and -14 T. Only the first quadrant (0 to 14 T) is plotted in Figure 8. No

coercive fields, exceeding 20 Oe, were found at 4 and 20 K in our experiments. Either at 4 and 20 K the magnetization saturates at around the same level, 146 Am^2/kg, when the magnetic field is applied along the *b*-axis (zero degree curves). This corresponds to a saturation magnetic moment of $6.9\mu_B$ per formula unit. The saturation magnetization diminishes gradually down to about 120 Am^2/kg as rotating the sample up to 80^o towards the *c* direction. The hereby observed 18 % reduction in magnetizations proves that magnetic anisotropy hinders a rotation of magnetic moments from the easy magnetic direction, i.e. the *b* axis. No magnetic irreversibility effect has been observed within the experimental accuracy by comparing FC and ZFC measurements (not shown here), whatever the magnetic field orientation, for the above magnetic field regimes. It is worth to notice that a reversible behaviour was similarly found [21] for a polycrystalline $DyMnO_3$.

A remarkably different behaviour is observed when the magnetic field is oriented along the *c*-axis (90^0 curves). A linear variation of the magnetization, as in paramagnetic regimes, is registered; no saturation is seen to be achieved up to the applied 14 T magnetic fields. The slope in linear variation of the magnetization is considerably lowered when varying a temperature from 4 to 20 K. This in turn, corresponds to a reduction in the magnetic susceptibility along the *c* axis. The corresponding highest magnetic moments in the 14 T magnetic field are $2.2\mu_B$ and $0.1\mu_B$ per formula unit at 4 and 20 K, respectively. A comparison of these magnetic moments along the *b* and *c* axes proves again that the *c* axis corresponds to the hard magnetic direction.

The magnetization isotherms (Figure 8) indicate a relatively abrupt magnetization increase at low fields. At magnetic fields about 5 T, applied at angles ranging from 0^o to 80^o with respect to the *b* axis, such a drop occurs at 4 K, where the magnetization curves approach saturation. On the other hand, at 20 K the magnetization curves approach saturation well above 10 T when the magnetic fields are oriented at angles between 0^o to 80^o.

Finally, in figure 9 we show that for B // *b*, as the temperature is raised from 3 to 10 K, a saturation magnetization can be achieved for "large" magnetic fields. At relatively weak fields, below 2 T, the magnetization curves exhibit inflection points, which suggest the spin flop type transition. The accurate magnetic field position of such inflection points B_{INF} has been determined by the maximum in dM/dB. It is found that this maximum weakens in magnitude and shifts down towards lower magnetic fields when raising the temperature (Figure 10). This spin flop transition disappears above 9 K as indicated by a dM/dB maximum located at B = 0. The relatively low magnetic fields (below 1.6 T) inducing such a spin flop transition reveal that there is a weak magnetocrystalline anisotropy stabilizing the antiferromagnetic ordering along the *b* axis. No spin flop transition is observed for magnetic fields parallel to the *c* axis.

7. Conclusion

An orthorhombic $DyMnO_3$ single crystal has been examined for its magnetic anisotropy in a broad temperature range and in magnetic fields up to 14 T. It is shown here that the magnetic field - temperature phase diagram is much dependent on the magnetic field orientation. The present observations are consistent with a picture assuming the sinusoidal incommensurate structure of Dy^{3+} magnetic moments along the *b* axis below 15 K [30]. Below T_N this structure changes to the antiferromagnetic one. At temperatures above the magnetization maximum, a typical paramagnetic Curie Weiss behavior is observed, which is related to some superposed Dy and Mn sublattice contributions, having different weight influence. This suggests that the antiferromagnetic Dy-Mn interaction and the ferromagnetic double exchange Mn-Mn interactions are weaker as compared with the Dy-Dy one. It is found that the easy and hard magnetic axes are oriented along the *b* and *c* axes, respectively. The antiferromagnetic structure is stabilized along the *b* axis by relatively weak magnetocrystalline anisotropy, as indicated by a spin flop transition induced below 9 K by

magnetic field up to 1.6 T. The excitations of Dy 4f electrons by the crystalline electric field may play a role in the matter, as suggested by Harikrishnan et al [18].

Further work may be here suggested. Experimentally, additional neutron diffraction study is required in order to better elucidate the magnetic microstructure. From a theoretical background, notice that the above description of the angle dependence of the Curie-Weiss parameters of T_W and μ_{EF} is here offered only as a first approximation. A more advance analysis should take into account the influence of the magnetocrystalline anisotropy itself, which is neglected in the classical isotropic (zero anisotropy) Curie-Weiss approach.

Acknowledgments
This work was supported in part by Ministry of Science and Higher Education (PL) and WBI (B) in a frame of scientific exchange agreement, and a bilateral agreement counterpart between the Bulgarian Academy of Sciences and University of Liege through the CGRI (BE). Experimental work at the NHMFL, Los Alamos National Laboratory, was supported by NSF, the U.S. Department of Energy, and the State of Florida. Experimental work at the Dresden High Magnetic Field Laboratory was supported by EuroMagNET II (EU Contract No. 228043). Authors are grateful to V. Drozd for helpful discussions.

References

[1] M. Bibes, A. Barthelemy, Nature Materials A, 7 (2008) 425.

[2] Y. Tokura, Report on Progress Physics 69 (2006) 797.

[3] S. Lee, A. Pirogov, J. H. Han, J.-G. Park, A. Hoshikawa, T. Kamiyama, Physical Review B 71 (2005) 180413.

[4] S.-W. Cheong, M. Mostovoy, Nature Materials 6 (2007) 13.

[5] T. Kimura, T. Goto, H. Shintani, K. Ishizaka, T. Arima, Y. Tokura, Nature 426 (2003) 55.

[6] J.-S. Zhou, J. B. Goodenough, Physical Review Letters 96 (2006) 247202.

[7] J.-S. Zhou, J. B. Goodenough, J. M. Gallardo-Amores, E. Morán, M. A. Alario-Franco, R. Caudillo, Physical Review B 74 (2006) 014422.

[8] N. Kamegashira, Y. Hiyoshi, Materials Letters 2 (1984) 337.

[9] Th. Lonkai, D. G. Tomuta, U. Amann, J. Ihringer, R. W. A. Hendrikx, D. M. Tobbens, J.

A. Mydosh, Physical Review B 69 (2004) 134108.

[10] J.A. Alonso, M.J. Martinez-Lope, M.T. Casais, M.T. Fernandez-Diaz, Inorganic Chemistry 39 (2000) 917.

[11] J. Strempfer, B. Bohnenbuck, M. Mostovoy, N. Aliouane, D.N. Argyriou, F. Schrettle, J. Hemberger, A. Krimmel, M. v. Zimmermann, Physical Review B 75 (2007) 212402.

[12] T. Kimura, G. Lawes, T. Goto, Y. Tokura, A.P. Ramirez, Physical Review B 71 (2005) 224425.

[13] A P Litvinchuk , M N Iliev , V N Popov, M M Gospodinov, Journal of Physics: Condensed Matter 16 (2004) 809.

[14] A. Munoz, J. A. Alonso, M. J. Martinez-Lope, M. T. Casais, J. L. Martinez, M. T. Fernandes-Diaz, Physical Review B 62 (2000) 9498.

[15] V. Skumryev, M.D. Kuz´min, M. Gospodinov, J. Fontcuberta, Physical Review B 79 (2009) 212414.

[16] A. Oleaga, A. Salazar, D. Prabhakaran, J.-G. Cheng, and J.-S. Zhou, Physical Review B 85, 184425 (2012)

[17] J. Macicek, 1988, Internal report of the Institute of Applide mineralogy, Bulg. Acad. Sciences, 36 pp.

[18] S. Harikrishnan, S. Roessler, C. M. Naveen Kumar, H. L. Bhat, U.K. Roessler, S. Wirth, F. Steglich, S. Elizabeth, Journal of Physics: Condensed Matter 21 (2009) 096002.

[19] V. Dyakonov, A. Szytuła, S. Baran, Z. Kravchenko, E. Zubov, O. Iessenchuk, W. Bazela, M. Dul, A. Zarzycki, H. Szymczak, Acta Physica Polonica A 117 (2010) 607.

[20] E.V. Milov, A.M. Kadomtseva, G.P. Vorobev, Yu.F. Popov, V.Yu. Ivanov, A.A. Mukhin, A.M. Balbashov, JETP Letters 85 (2007) 503.

[21] T. Mori, K. Aoki, N. Kamegashira, T. Shishido, T. Fukuda, Materials Letters 42 (2000) 387.

[22] Y. Wang, X. Lu, Y. Chen, F. Chi, S. Feng, X. Liu, Journal of Solid State Chemistry 178 (2005) 1317.

[23] S. Jandl, S.Mansouri, A.A.Mukhin, V.YuIvanov, A.Balbashov, M.M.Gospodinov, V. Nekvasil, M.Orlita, Journal of Magnetism and Magnetic Materials 323 (2011) 1104–1108.

[24] M. F. Hundley, J. J. Neumeier, Physical Review B 55 (1997) 11511.

[25] O. Pena, M. Bahout, D. Gutierrez, P. Duran, C. Moure, Solid State Sciences 5 (2003) 1217.

[26] R. I. Joseph, Journal of Applied Physics 38 (1967) 2405.

[27] A. Aharoni, Journal of Applied Physics 83 (1998) 3432.

[28] D.-X. Chen, E. Pardo, A. Sanchez, IEEE Transactions on Magnetics 38 (2002) 1742.

[29] D.-X. Chen, E. Pardo, A. Sanchez, IEEE Transactions on Magnetics 41 (2005) 2077.

[30] O. Prokhnenko, R. Feyerherm, E. Dudzik, S. Landsgesell, N. Aliouane, L.C. Chapon, D.N. Argyriou, Physical Review Letters 98 (2007) 057206.

[31] I.O. Troyanchuk, V.N. Derkachenko, S.S. Korneeva, O.A. Novitski, Soviet Physics Solid State 34 (1992) 48.

Figures

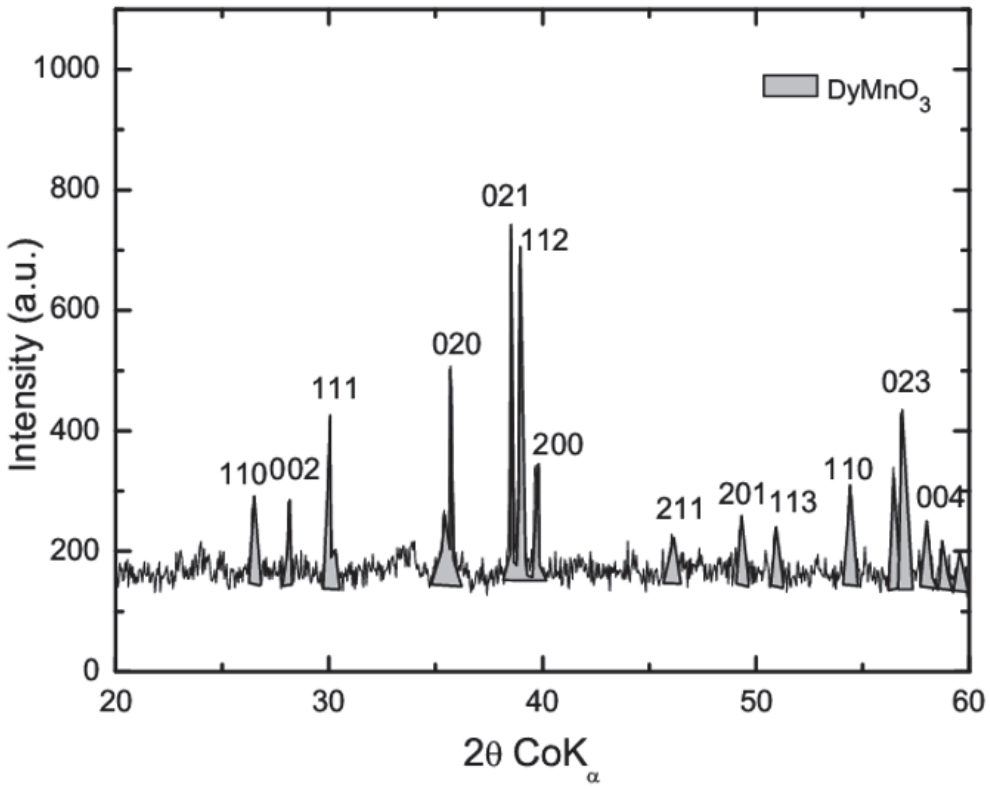

Figure1. X-ray diffraction pattern for a $DyMnO_3$ single crystal.

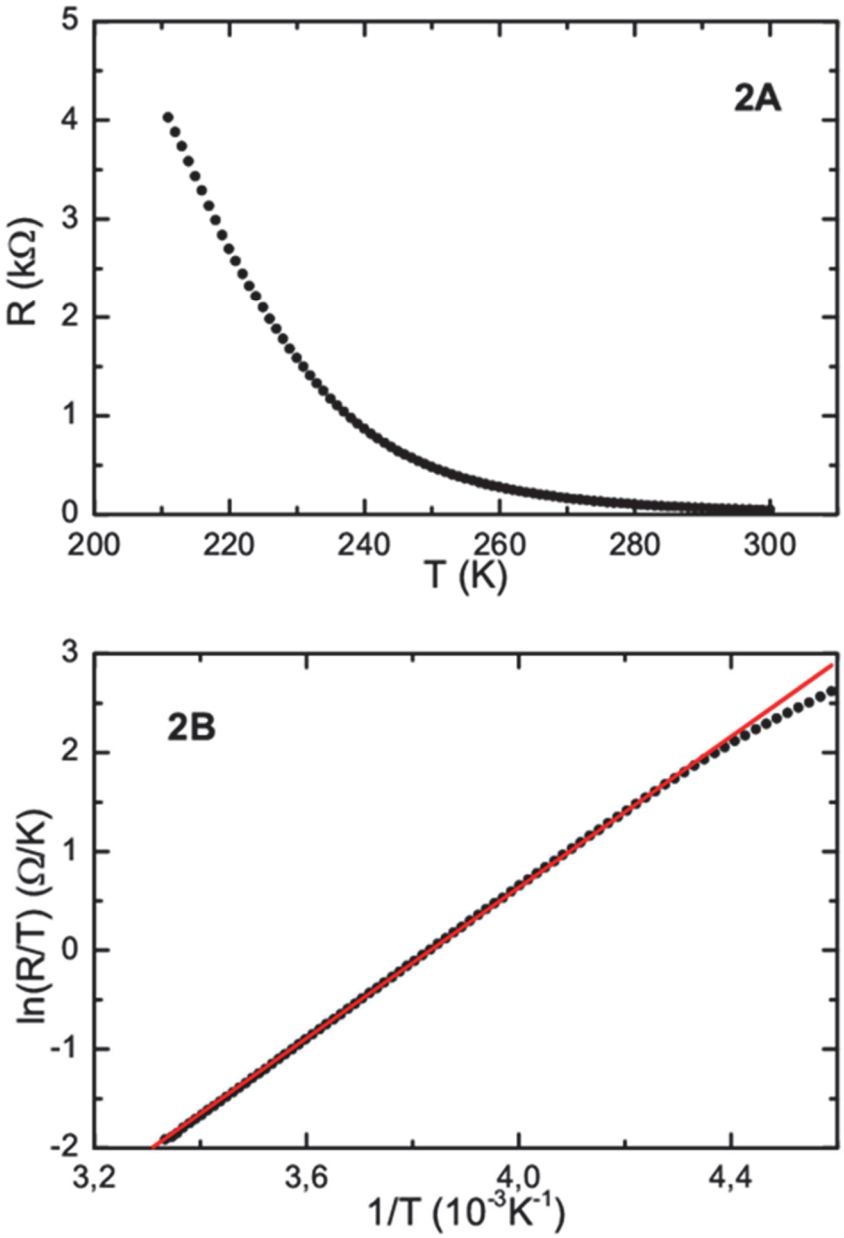

Figure 2. Panel 2A shows the electrical resistance as function of temperature and panel 2B shows a plot of ln(R/T) vs 1/T with the straight line fitting to the the polaron conduction mechanism.

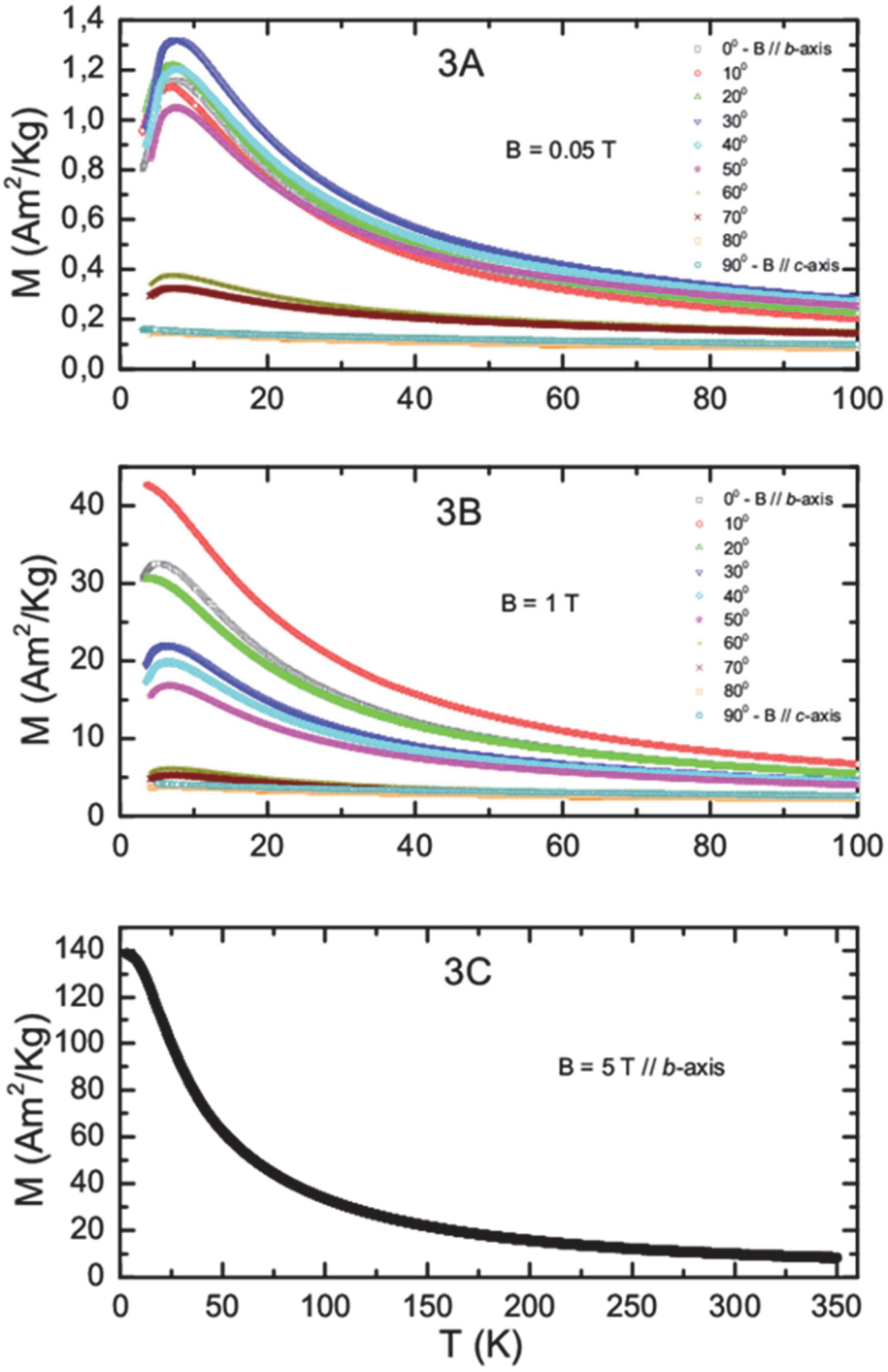

Figure 3. Temperature dependence of the $DyMnO_3$ single crystal magnetization at 0.05 T (panel 3A), 1 T (panel 3B) and 5 T (panel 3C) for different orientations. Sequence of curves from top to bottom corresponds to magnetic field orientation from the *b* (0^0) to *c* (90^0) axis.

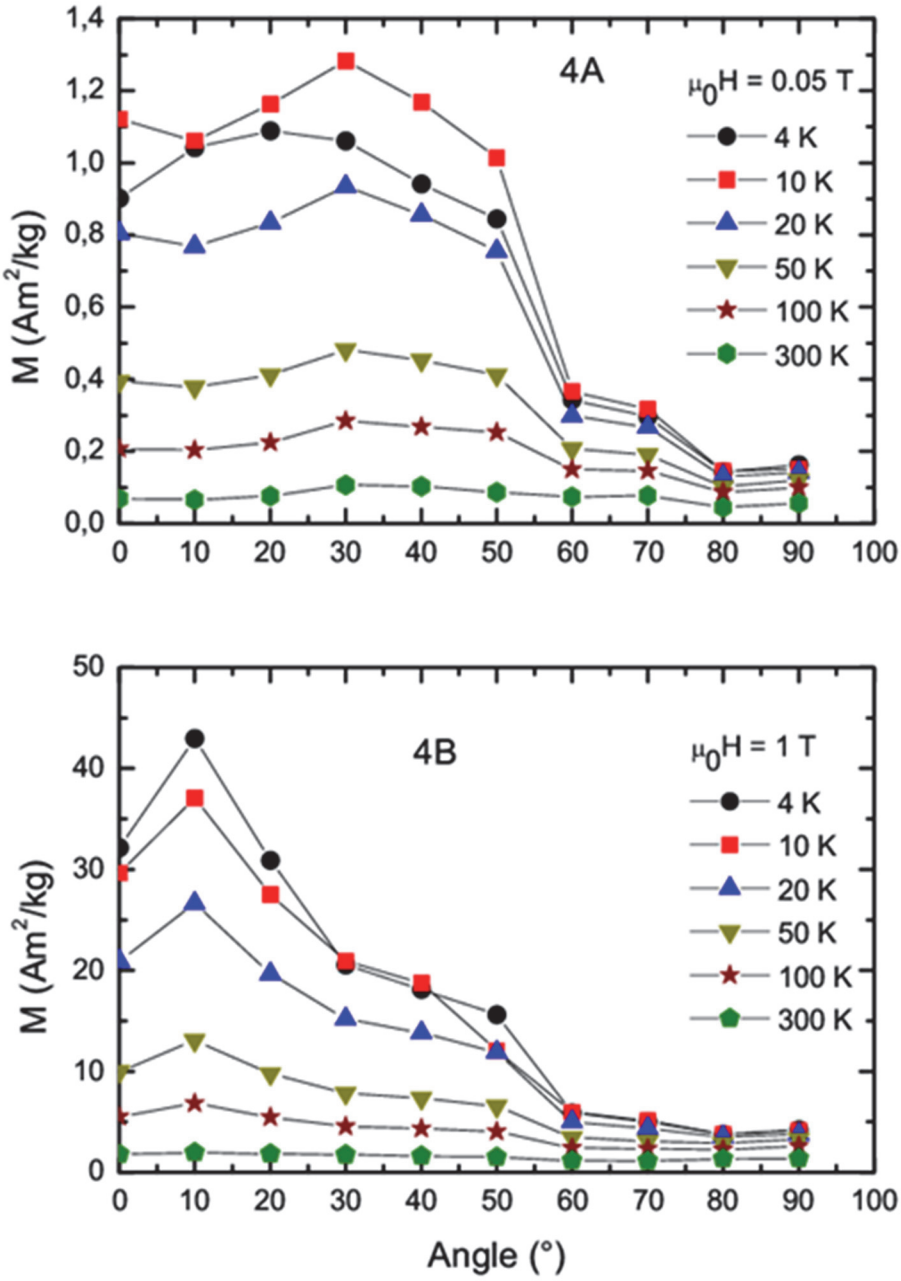

Figure 4. Dependence of the $DyMnO_3$ single crystal magnetization as a function of sample orientation from the *b* (0^0) to *c* (90^0) axis, measured at selected temperatures and at 0.05 T (panel 4A) and 1 T (panel 4B).

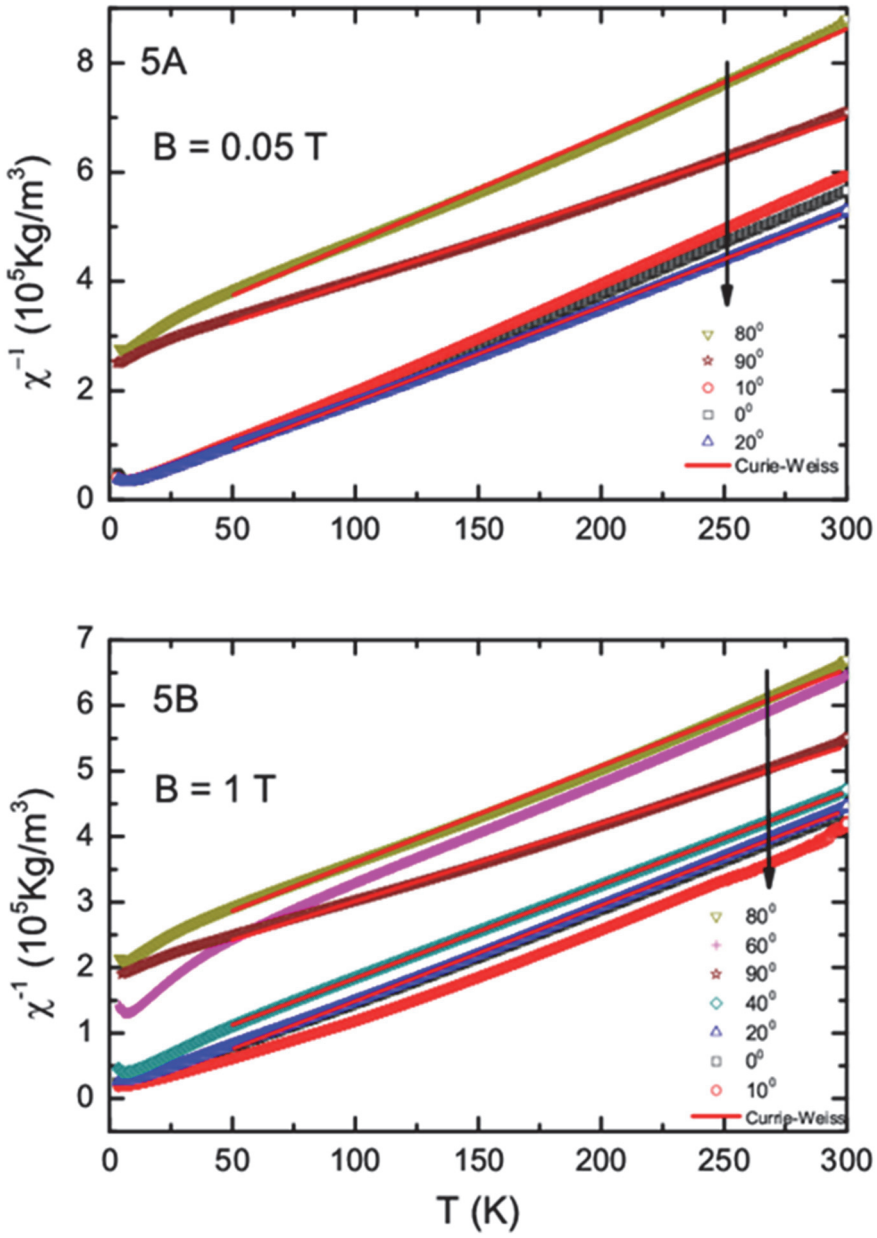

Figure 5. Temperature variation of the inverse magnetic susceptibility of the $DyMnO_3$ single crystal at 0.05 T (panel 5A) and 1 T (panel 5B) for some of measured magnetic field orientations. Other (overlapping) curves are omitted for the sake of clarity.

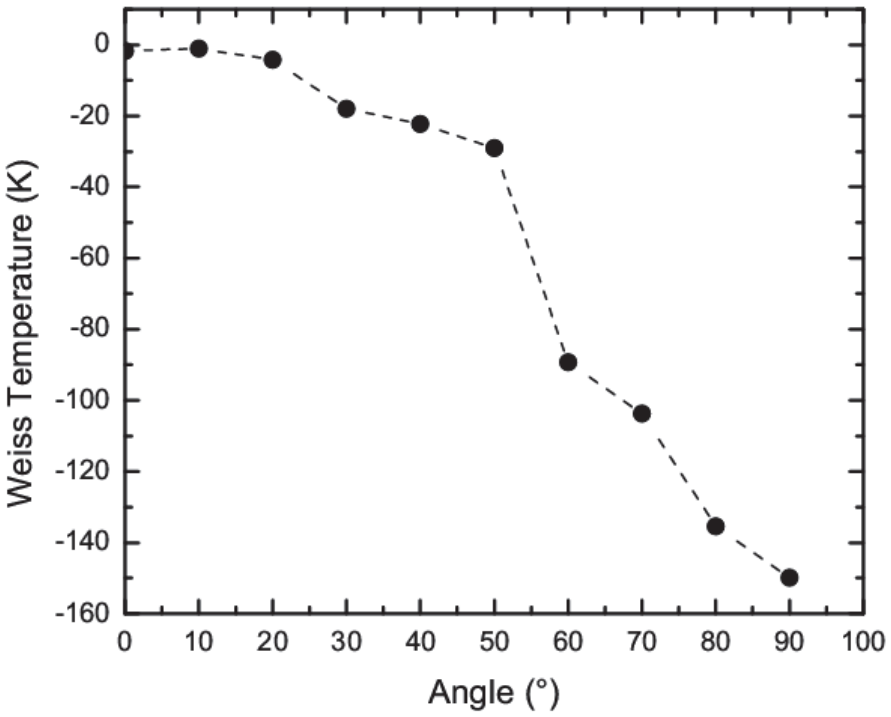

Figure 6. Weiss temperature as a function of magnetic field orientation rotated from the *b* (0^0) to *c* (90^0) axis for a $DyMnO_3$ single crystal. Line only guides the eye.

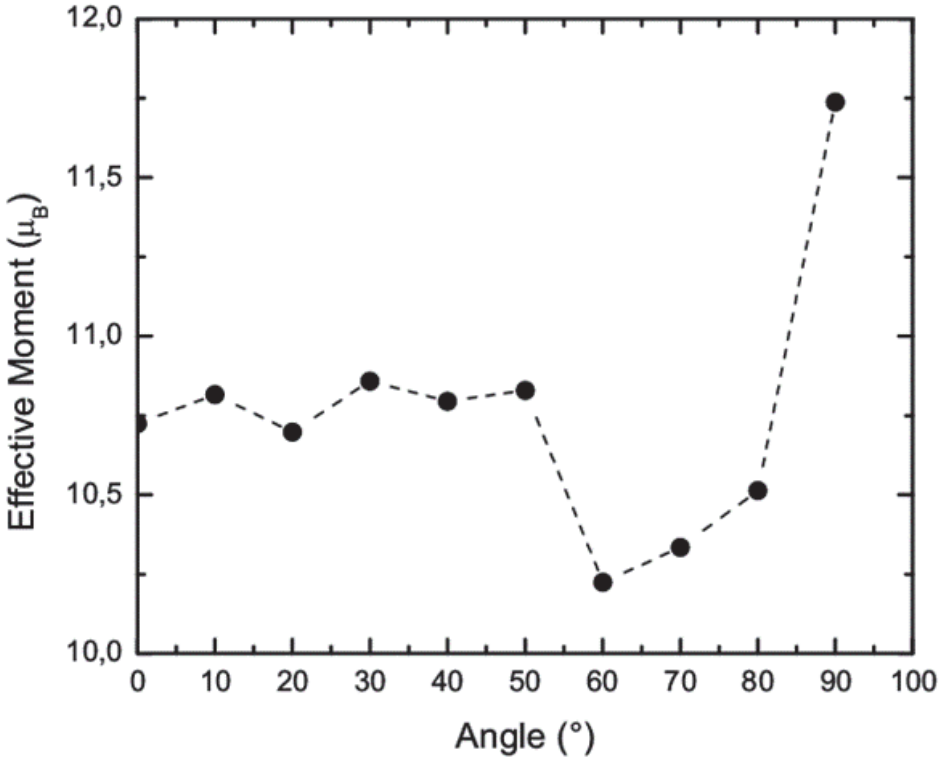

Figure 7. The effective magnetic moment as a function of magnetic field orientations from the *b* (0^0) to *c* (90^0) axis for a $DyMnO_3$ single crystal. Line only guides the eye.

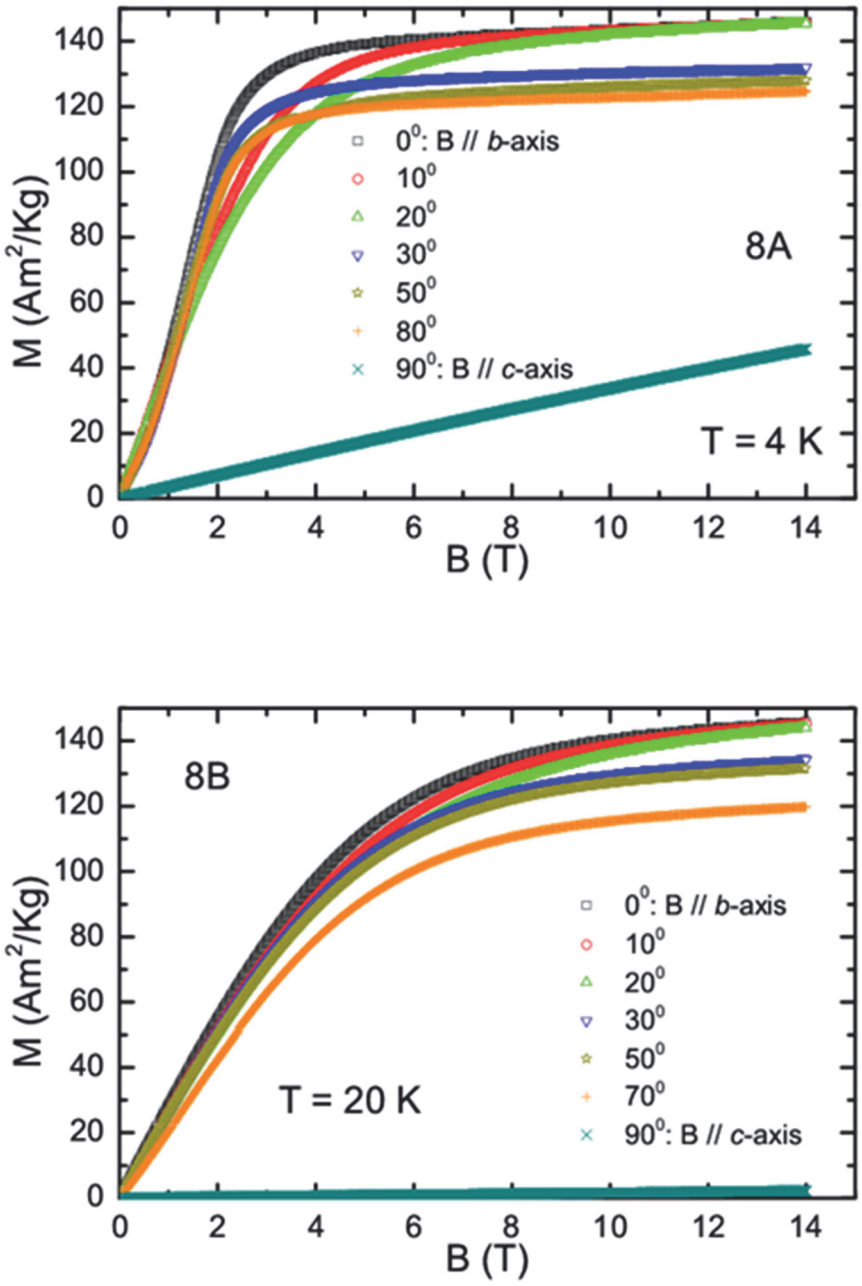

Figure 8. Magnetization of a $DyMnO_3$ single crystal as a function of the magnetic field for different magnetic field orientations rotated from the *b* (0^0) to *c* (90^0) axis, measured at 4 K (panel 8A) and 20 K (panel 8B). Sequence of curves from top to bottom corresponds to magnetic field orientation from the *b* (0^0) to *c* (90^0) axis.

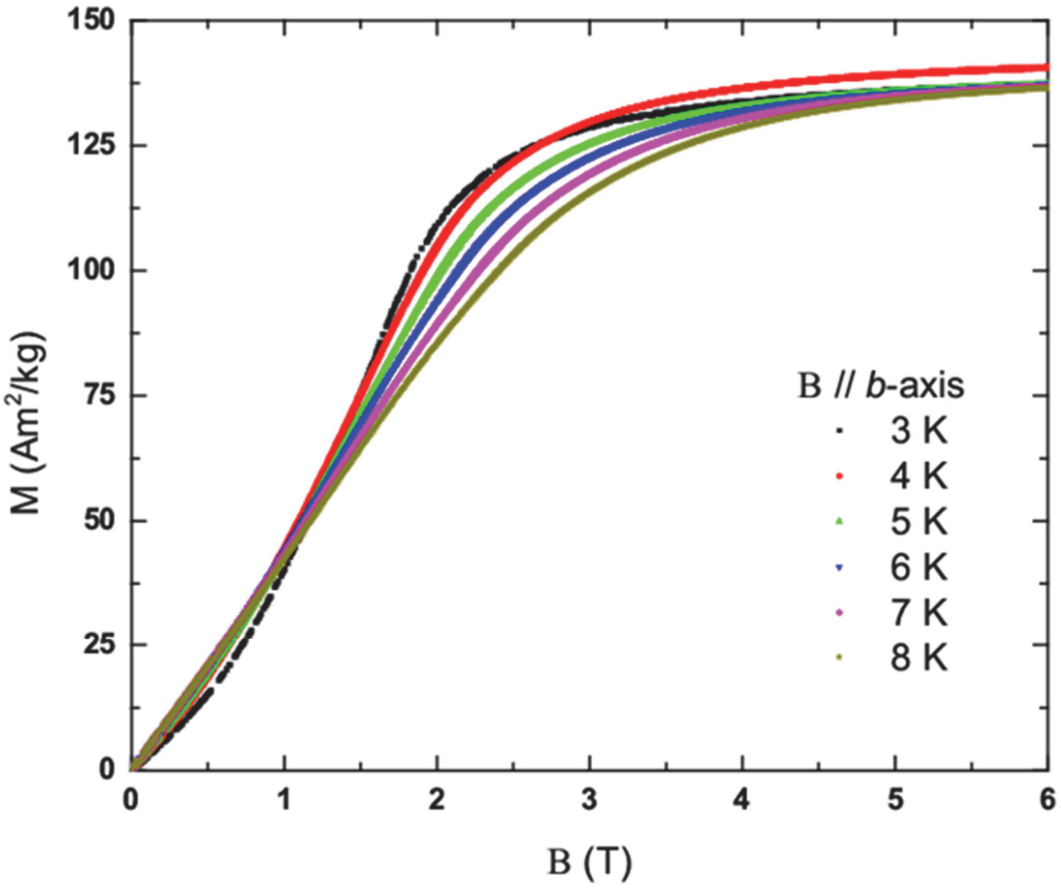

Figure 9. Magnetization of a $DyMnO_3$ single crystal as a function of magnetic field B applied along the *b* axis for some of the measured temperatures.

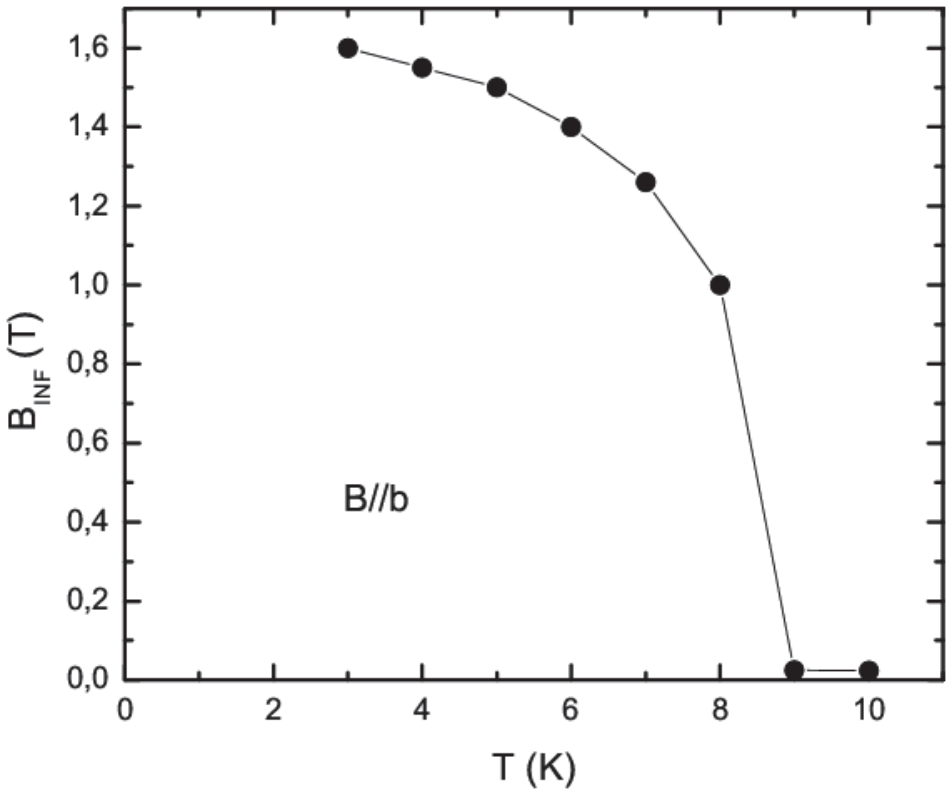

Figure 10. Temperature dependence of the magnetic field inflection point B_{INF} (from figure 9) at which the spin flop transition occurs in a $DyMnO_3$ single crystal when the magnetic field is oriented along the *b* axis.